JOURNAL OF AIRCRAFT
Vol. 45, No. 4, July–August 2008

Performance and Flow Characteristics of Double-Offset Y-Shaped Aircraft Intake Ducts

Rajesh K. Singh,* S. N. Singh,† and V. Seshadri‡
Indian Institute of Technology Delhi, New Delhi 110 016, India

DOI: 10.2514/1.34137

A Y-shaped intake duct is a critical component of a single-engine modern combat aircraft. The present study is an attempt to establish the flow behavior of a double-offset Y duct with uniform wall roughness with a semi-elliptical inlet and a circular exit. These studies are carried out using the commercial computational fluid dynamics code FLUENT with a renormalized-group k-ε turbulence model. An attempt was made to establish the effect of Reynolds number and vertical offset on the flow characteristics of a double-offset Y duct for a fixed horizontal offset. It is seen that performance and flow characteristics of the duct are independent of Reynolds number for $Re > 10^5$. In the presence of a vertical offset, the core of the flow moves along the diagonal plane, which is inclined to the vertical axis at an angle determined by the magnitude of the vertical offset (a 15/15-deg offset gives an angle of 30 deg).

Nomenclature

A_R	=	area ratio, A_o/A_i
A_s	=	aspect ratio
C_L	=	coefficient of total pressure loss
C_P	=	coefficient of pressure recovery
$C_{1\varepsilon}$, $C_{2\varepsilon}$, C_∞	=	model constants
D_H	=	inlet hydraulic diameter of the Y duct
D_o	=	outlet diameter of the duct
DC_{60}	=	distortion coefficient
F_i	=	external body force
G_k	=	generation of turbulent kinetic energy due to mean velocity
I	=	turbulent intensity, $0.16(Re)^{-1/8}$
i, j, k, l	=	tensorial notations
i	=	inlet
k	=	turbulent kinetic energy, m^2/s^2
L	=	length of the duct, characteristic length
M	=	freestream Mach number
o	=	outlet
p	=	static pressure, Pa
R_H	=	radius of curvature (horizontal)
R_V	=	radius of curvature (vertical)
S_k, S_ε	=	user-defined source terms for k and ε
S_m	=	mass added to continuous phase
u_{yz}	=	crossflow at the exit, m/s
u_∞	=	mean inlet velocity, m/s
V_e	=	average exit velocity, m/s
V_{yz}	=	secondary flow
X	=	axial position
x, r	=	axial and radial directions
α_k, α_ε	=	inverse effective Prandtl number for k and ε
δ_{ij}	=	Kronecker's delta
ε	=	turbulent kinetic energy dissipation rate, m^2/s^3
μ	=	molecular viscosity
μ_{eff}	=	effective viscosity, $\mu_{\text{eff}} = \mu + \mu_t$
μ_t	=	turbulent or eddy viscosity
ρ	=	density of fluid
σ_k, σ_ε	=	Prandtl number for k and ε

Received 20 August 2007; revision received 7 February 2008; accepted for publication 10 February 2008.

*Graduate Student, Department of Applied Mechanics; rajeshsingh.175@gmail.com.

†Professor, Department of Applied Mechanics; sidhnathsingh@hotmail.com. Member AIAA (Corresponding Author).

‡Professor, Department of Applied Mechanics; vs@am.iitd.ac.in.

I. Introduction

MODERN fighter aircraft have a single engine with a lower number of compressor stages, with each possessing a higher pressure ratio. The performance of the compressor is highly sensitive to the flow quality at the exit of the air-intake duct (inlet of the compressor). The intakes for the fighter aircraft are mounted at various locations of the air frame structure: namely, side-mounted on the fuselage (M2000 and JAS 39), fuselage shield (F-16 and European fighter aircraft), wing shield (F18 and light combat aircraft), etc. From the point of view of space constraint and aerodynamics, a short intake is desirable, to minimize the losses while maintaining the mass flow requirements of the engine. The intake for the combat aircraft must meet the engine mass flow requirement with steady and symmetric conditions over a wide range of aircraft speeds and altitudes, ensuring higher pressure recovery with minimum distortion in the flow at the inlet of the compressor [1]. For the single-engine modern combat aircraft, the fuselage-mounted Y-shaped intake ducts are widely used. These consist of two limbs merging into a single duct ahead of the compressor. Basically, these limbs are S-shaped ducts with a semicircular outlet merging into a circular pipe and providing greater flexibility to ensure diffusion over shorter lengths. The flow in these ducts is quite complex as a result of simultaneous turning and diffusion, which causes the flow distortion and creates strong secondary flows at the exit.

Systematic and extensive experiments were carried out by various researchers [2–10] to understand the flow characteristics of the Y ducts. One of the pioneer works reported is that of Martin and Holzhauser [2], who conducted experiments for the determination of pressure recovery and drag characteristics of a NACA submerged intake with deflector installation on the rear portion of the fuselage. The same authors [3] also conducted experiments to understand the flow instability in the Y duct at a low inlet velocity ratio for various intake configurations and showed that flow instability and flow reversal are a function of static pressure recovery. Jolly et al. [4] explained the flow instability phenomenon of buzz and pulse in the Y duct and they investigated the effect of fuselage protuberance on buzz. A design methodology for the intake duct was discussed by Pai [5] for interrelated design objectives of Y-shaped intake ducts: namely, intake airframe integration and engine intake compatibility. Further, he also showed the complex nature of the interaction between internal and external flows in a modern combat aircraft.

Sudhakar and Ananthkishnan [6] explained the jump phenomenon due to the transition of symmetric to asymmetric operation in the Y duct in supersonic flight. Obery and Cubbison [7] studied the effect

of the boundary-layer removal inside the inlet on the performance of a twin supersonic intake duct. They observed increased pressure recovery and higher propulsive thrust after the partial removal of the boundary layer. Obery and Stitt [8] conducted experiments to investigate the performance of a twin-intake duct with a 9-deg compressor ramp for a supersonic aircraft in the same range of Mach number. They also investigated the effect of boundary-layer removal by a wedge and the main duct bypass system.

Davis and Goldstein [9] investigated the effect of a slot on the performance of a twin-scoop supersonic air-intake duct and found more stable local flow and higher total pressure after diffusion than with the inlet without a slot. They also observed that the ramp angle producing the maximum total pressure recovery is greater for a slotted duct entrance than for the inlet without slots. Davids and Wise [10] carried out experiments for performance improvements of a supersonic twin-intake duct using a two-dimensional compression ramp and found minor changes in the flow characteristics. Seddon and Goldsmith [11] studied the inlet flow separation due to frictional loss on the fuselage surface. A mathematical formulation for quantifying the flow distortion at the compressor inlet was proposed.

Bharani et al. [12,13] investigated the flow characteristics of a Y duct for incompressible flow using computational fluid dynamics (CFD) and observed four pairs of counter-rotating vortices at the merger plane. They also established the effect of area ratio, inlet Reynolds number, and angle of turn on the performance of Y duct. Patel et al. [14] investigated the effect of inflow condition on the performance of a Y duct and observed a reduction in the static pressure recovery with increase in the skewness of velocity profile at the inlet of one of the limbs. Saha et al. [15] used CFD to examine the impact of inlet shape on the performance of a Y duct and showed that the semi-elliptical inlet duct gives a better performance. Singh et al. [16] studied the flow characteristics of a double-offset circular S duct for various horizontal offsets for a fixed vertical offset of 22.5/22.5 deg (angle of turn in the vertical plane) using the renormalized-group (RNG) k-ε model and showed that a horizontal offset of 15/15 deg (angle of turn in the horizontal plane) gives a comparatively better performance.

A review of the literature gives insight into the utility of CFD as a tool for the study of complex flows, and it can be exploited further. The scope of the present work is to establish the effect of Reynolds numbers and angle of turn on the performance of a double-offset Y duct. The flow is assumed to be incompressible, because this has been observed to be adequate to understand the fluid dynamic characteristics of subsonic intakes [11].

II. Mathematical Formulation

CFD involves the numerical solution of governing equations of fluid flows that are obtained by invoking basic laws. The governing equations for steady incompressible flows are

$$\frac{\partial}{\partial x_i}(\rho u_i) = S_m \tag{1}$$

$$\frac{\partial}{\partial x_j}(\rho u_i u_j) = -\frac{\partial p}{\partial x_i} + \frac{\partial}{\partial x_j}\left[\mu\left(\frac{\partial u_i}{\partial x_j} + \frac{\partial u_j}{\partial x_i} - \frac{2}{3}\frac{\partial u_i}{\partial x_i}\delta_{ij}\right)\right] + \rho g_i + F_i \tag{2}$$

Most of the practical flows are turbulent, which is characterized by the fluctuations of flow variables around a time-averaged mean value [17]. Introducing this fact in the Navier–Stokes equation leads to Reynolds-averaged Navier–Stokes equations, as follows:

$$\rho u_j \frac{\partial u_i}{\partial x_j} = -\frac{\partial p}{\partial x_i} + \frac{\partial}{\partial x_j}\left[\mu\left(\frac{\partial u_i}{\partial x_j} + \frac{\partial u_j}{\partial x_i}\right) - \frac{2}{3}\mu\delta_{ij}\frac{\partial u_i}{\partial x_i}\right] + \frac{\partial}{\partial x_j}(-\overline{\rho u_i' u_j'}) \tag{3}$$

These equations are the same as the basic equations, except for additional terms in each momentum equation. The additional terms in the preceding equations are the Reynolds stresses and need to be modeled for closure. Boussinesq hypothesis is used to relate the Reynolds stresses to the mean velocity gradient, as follows [17]:

$$-\overline{\rho u_i' u_j'} = \mu_t\left(\frac{\partial u_i}{\partial x_j} + \frac{\partial u_j}{\partial x_i}\right) - \frac{2}{3}\left(\rho k + \mu_t\frac{\partial u_i}{\partial x_i}\right) \tag{4}$$

where μ_t is the eddy viscosity, k is the turbulent kinetic energy, and δ_{ij} is Kronecker's delta.

A two-equation RNG k-ε turbulence model was used that is expected to be superior to the standard k-ε model for the analysis of separated flows and for flows with high streamline curvature and rapid strain (Yakhot and Orszag [18]). The RNG k-ε turbulence model is similar to the standard K-ε model, except for an additional term in the dissipation equation that improves the prediction capabilities for these kinds of flows. The model equations are

$$\rho u_i \frac{\partial k}{\partial x_i} = \frac{\partial}{\partial x_i}\left[\alpha_k \mu_{\text{eff}}\frac{\partial k}{\partial x_i}\right] + G_k - \rho\varepsilon \tag{5}$$

$$\rho u_i \frac{\partial \varepsilon}{\partial x_i} = \frac{\partial}{\partial x_i}\left[\alpha_\varepsilon \mu_{\text{eff}}\frac{\partial \varepsilon}{\partial x_i}\right] + C_{1\varepsilon}\frac{\varepsilon}{k}(G_k) - C_{2\varepsilon}\frac{\rho\varepsilon^2}{k} - R \tag{6}$$

where G_k is the generation of turbulent kinetic energy due to the mean velocity gradient and is calculated as

$$G_k = \mu_t S^2 \tag{7}$$

S is the mean rate of shear stress tensor, defined as

$$S = \sqrt{2S_{ij}S_{ij}} \tag{8}$$

where

$$S_{ij} = \frac{1}{2}\left(\frac{\partial u_i}{\partial x_j} + \frac{\partial u_j}{\partial x_i}\right)$$

$C_{1\varepsilon}$ and $C_{2\varepsilon}$ are constants, and α_k and α_ε are the inverse of effective turbulent Prandtl numbers for the k and ε equations, respectively. The effective viscosity is modeled in the RNG theory using the scale-elimination procedure, resulting in a differential equation for turbulent viscosity, as follows:

$$d\left(\frac{\rho^2}{\sqrt{\varepsilon\mu}}\right) = 1.72\frac{\hat{\nu}}{\sqrt{\hat{\nu}^3 - 1 - c_\nu}}\,\mathrm{d}\hat{\nu} \tag{9}$$

where

$$\hat{\nu} = \frac{\mu_{\text{eff}}}{\mu} \qquad c_\nu \cong 100$$

At high Reynolds numbers, the preceding equation gives

$$\mu_t = \rho C_\mu \frac{k^2}{\varepsilon} \tag{10}$$

The additional rapid strain term R in the dissipation equation is

$$R = \frac{C_\mu \rho \eta^3 (1 - \eta/\eta_0)}{1 + \beta\eta^3}\frac{\varepsilon^2}{k} \tag{11}$$

where $\eta = S \cdot k/\varepsilon$. The values of constants in the turbulence model used are the standard values suggested by Yakhot and Orszag [18]: $C_{1\varepsilon} = 1.42$, $C_{2\varepsilon} = 1.68$, $C_\mu = 0.0845$, $\alpha_k = \alpha_\varepsilon = 0.7179$, $\eta_0 = 4.38$, and $\beta = 0.012$.

Proper modeling of the near-wall region is a vital step for wall-bounded turbulent flows because viscous effects are pronounced in this region. Near-wall regions were modeled with a standard wall function for the equilibrium turbulent boundary layer. In the equilibrium turbulent boundary layer, Y^+ and Y^* have same values

[19] and are given as

$$Y^* = \frac{C_\mu^{1/4} k^{1/2} Y}{\nu} \qquad u^* = \frac{C_\mu^{1/4} U k^{1/2}}{\tau_w/\rho}$$

where $u_\tau = C_\mu^{1/4} k^{1/2}$. The effect of roughness is incorporated by the roughness constant, and the velocity profile is given as

$$\frac{U u^*}{\tau_w/\rho} = \frac{1}{K} \ell_n \left(E \frac{u^* y_p}{\nu} \right) - \Delta B \tag{12}$$

where $K = 0.41$, $\Delta B = 5$, and y_p is the roughness height, taken as 1.0 mm.

Flow simulations were carried out using the CFD code FLUENT [20], which is based on a cell-centered finite volume approach. A segregated solver and an implicit solution scheme in conjunction with an algebraic multigrid method were used for faster convergence. The second-order upwind scheme was used in the discretization scheme for all equations to ensure higher accuracy. Coupling between velocity and pressure was established by a semi-implicit method for pressure-linked equations (SIMPLE) algorithm [21]. Under-relaxation factors were used for all equations to satisfy the Scarborough condition for convergence. Convergence of the solution was assumed when the sum of normalized residual for each conservation equation was less than or equal to 10^{-8}. The residuals for different equations are defined as

$$\frac{\sum_{i=1}^{M} |R_i|^2}{S_{N\phi}} \leq 10^{-8} \tag{13}$$

Computations were made on a Intel Xeon processor with 2-GB RAM and a Silicon Graphics workstation. A typical grid size of 750,000 nodes takes around 12 h for a converged solution.

III. Validation

CFD has emerged as an effective alternative to the experimental studies for the parametric investigation after the validation of the code against the experimental results. Validation of the code shows the extent of reliability of the parametric investigation. For this purpose, preliminary investigations were carried out for validation of the CFD code against the experimental results of Anand [22] for the S duct with 22.5/22.5-deg angle of turn and $A_R = 2.0$. The schematic layout of the geometry of the S duct is shown in Fig. 1.

Flow predictions were carried out for this flow geometry with different turbulence models. The geometry modeled has uniform roughness of 1.0 mm and it was also specified in the wall-boundary conditions. Figure 2a shows the comparison between the predicted and experimental C_P along the longitudinal direction of the diffuser for different turbulence models. The trend of predicted C_P is similar to experimental results for all turbulence models, but the RNG k-ε model gives the closest match. The variation of the C_P is almost the same up to one-quarter of the duct, but beyond that, the predicted C_P values are higher than the experimental values.

Figure 2b shows the comparison of the normalized axial velocity contours at the exit of the duct. CFD-predicted results have a smaller core region near the convex wall than in the experimental results, but the match in the core region is reasonably good. Hence, it can be said that predictions made using the CFD code FLUENT with the RNG k-ε turbulence model match reasonably well with experimental results, both qualitatively and quantitatively, within acceptable limits. Minor deviations could be attributed to the limitations of the turbulence model in regions of high-velocity gradient, surface roughness of the test diffuser, and uncertainty in experiments. Hence, it is assumed that the solution methodology was validated and it can be used for further parametric investigations using the RNG k-ε turbulence model.

IV. Geometries Investigated

Flow analyses were carried out to understand the flow characteristics of a double-offset Y-shaped aircraft intake duct and the effect of the vertical offset on its performance. Horizontal and vertical offsets were defined in terms of angle of turn. The geometry of the double-offset Y duct consists of two limbs with a fixed horizontal offset of 22.5/22.5, as suggested by Bharani et al. [13]. Three vertical offsets (namely, 15/15, 22.5/22.5, and 30/30 deg) were used for three geometries. The radii of curvature for these three vertical offsets were 504, 382, and 252 mm, respectively, whereas the radius of curvature for a fixed horizontal offset was 382 mm. The centerline length of all ducts was 300 mm, which falls under the category of a short-diffusing duct. The inlet shape of each limb was chosen as semi-elliptical because it gives a better performance for a single-offset Y duct (Saha et al. [15]). The semi-elliptical inlet has a semimajor axis of 64 mm and a semiminor axis of 50 mm, which gives a hydraulic diameter of 71.70 mm.

Corners at the inlet were rounded with a 10-mm arc radius to overcome the effect of sharp corners. The exit of each limb was a semicircular shape ($\phi = 160$ mm), which merged into a common circular duct of equal diameter and length of $5D$. This length was incorporated to ensure the proper specification of the pressure-outlet boundary condition. Based on these parameters, the overall area ratio of each Y duct was 2.0. Each limb of the duct was created per the design methodology given by Fox and Kline [23]. The schematic layout of the Y duct is shown in Fig. 3.

The 3-D geometry of the double-offset Y-shaped intake duct was created with an initial vertex to the final volume using GAMBIT, which is the CAD tool of the CFD code FLUENT. A grid was also generated in the same fashion, starting from face meshing to final-volume meshing. The inlet face of the limb was meshed into two parts: boundary-layer meshing near the wall region and body-fitted nonorthogonal meshing in the core region. Boundary-layer meshing was used to capture the effect of steep velocity gradients close to the wall region. Side faces and the outlet of the Y duct were also meshed with the same type of mesh. Thereafter, flow volume was meshed with the body-fitted hexahedral cooper meshing, which gives a better result and economy in computation. The 3-D discretized model of the flow domain is shown in Fig. 4.

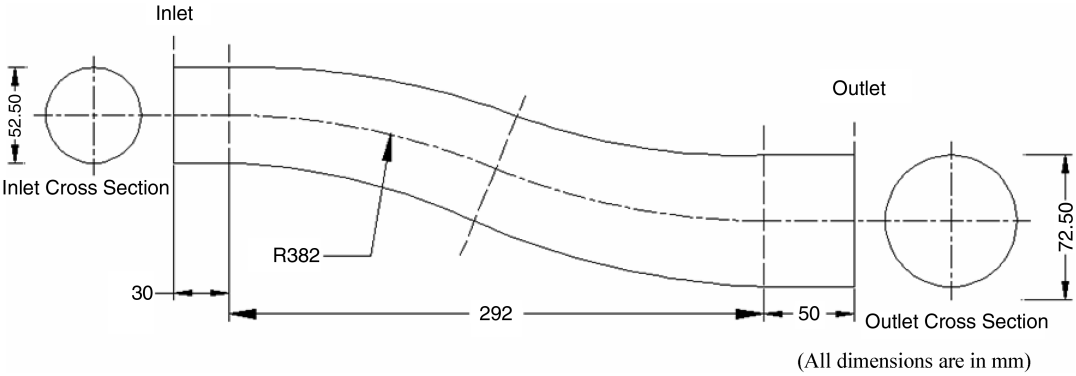

Fig. 1 Schematic layout of the geometry of an S duct used for validation [22].

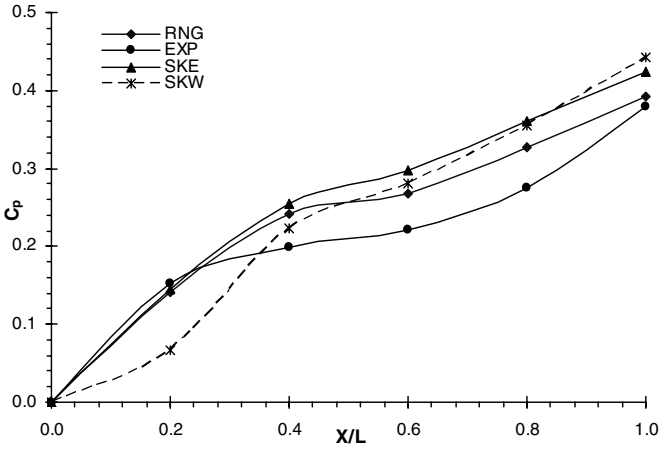

a) Comparison of predicted pressure recovery coefficient with experimental results [22]

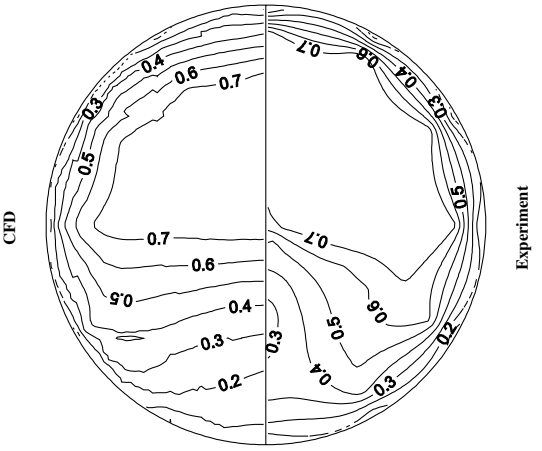

b) Comparison of predicted and experimental longitudinal velocity distribution [22] at the exit

Fig. 2 Comparisons of predicted and experimental results [22] for a) pressure-recovery coefficient and b) longitudinal velocity distribution at the exit (RNG is the RNG k-ε turbulence model, EXP is the experiments, SKE is the standard k-ε turbulence model, and SKW is the standard k-ω turbulence model).

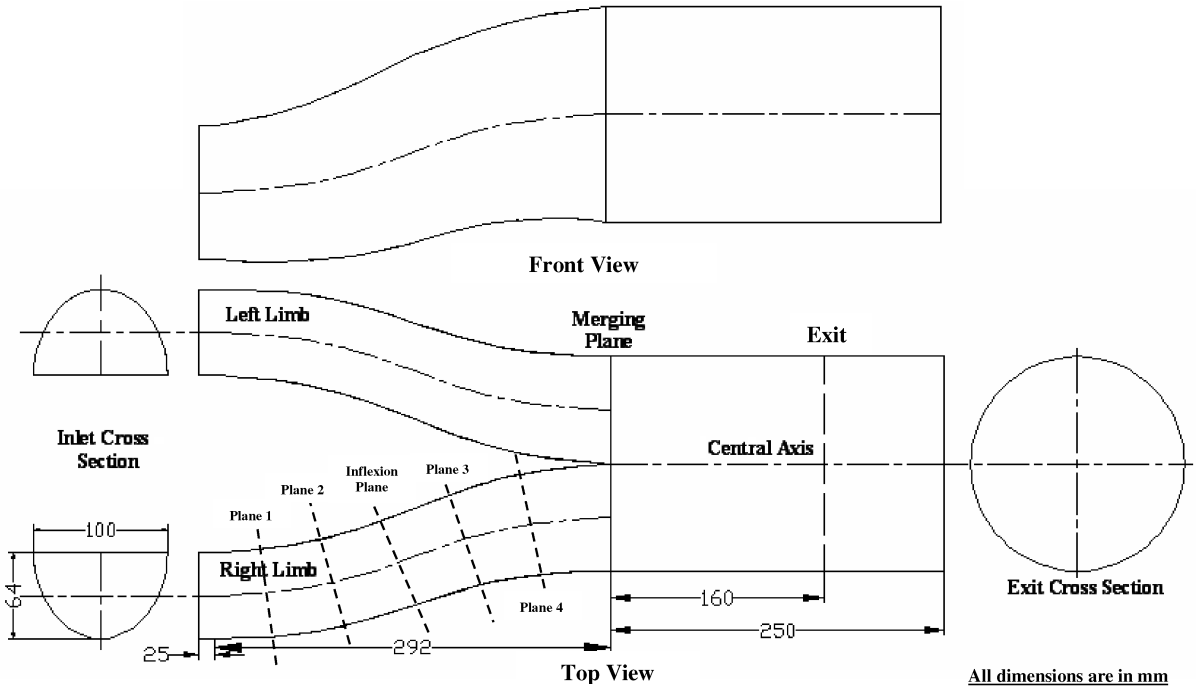

Fig. 3 Schematic layout of the Y duct showing double offsets.

Subsequently, the grid independency test was also carried out to get the optimum number of cells for every flow model. For the sake of brevity, these results are not presented here. During the simulation, a grid adaptation scheme was also performed in the regions of high-velocity gradient and reverse flow to capture the flow features. Table 1 shows the details of the meshing scheme, number of meshes, and nodes used for simulations.

CFD simulations were carried out for a uniform velocity at the inlet, with air at 30°C as the working fluid ($\rho = 1.16$ kg/m^3 and $\mu = 1.84 \times 10^{-5}$ kg/ms). The exit of the flow domain was specified as the pressure outlet with zero gauge pressure. Remaining boundaries of the flow domain are specified as the wall with a standard wall function. The roughness height of the wall was specified as 1.0 mm, with a roughness constant of 0.5. Turbulence intensity I computed from the relation $I = 0.16(Re)^{-1/8}$ and hydraulic diameter D_H are specified at the inlet for initialization of the turbulent quantities k and ε and are computed as

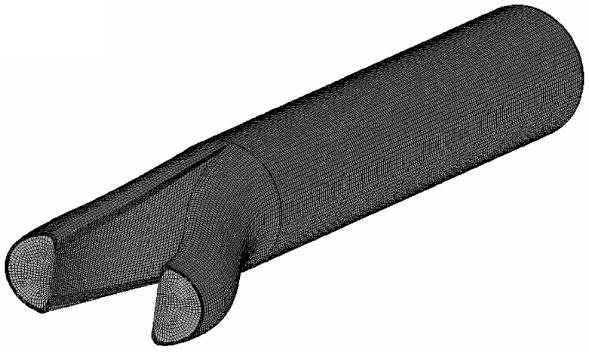

Fig. 4 Discretized 3-D geometry of one of the double-offset Y ducts.

Table 1 Details of geometry and discretization for double-offset Y ducts with a fixed horizontal offset of 22.5/22.5 deg

Serial no.	Vertical offset	Radius of curvature	Number of grids	Number of nodes
1	No offset	Nil	631,236	732,610
2	15/15 deg	573 mm	797,713	885,742
3	22.5/22.5 deg	382 mm	878,596	940,141
4	30/30 deg	286 mm	1,151,896	1,252,098

$$k = \frac{3}{2}(u_{av}I)^2 \qquad \varepsilon = C_\mu^{3/4}\frac{K^{3/2}}{l}$$

where $l = 0.07L$.

V. Results and Discussion

CFD predictions were carried out to investigate the flow and the performance characteristics of a double-offset Y-shaped aircraft intake duct. Results for the normalized axial velocity and the crossflow distribution at various selected planes of the duct are presented (see Fig. 3). The performance parameters of the Y duct were also evaluated in terms of pressure recovery, pressure-loss coefficient, and the distortion coefficient.

A. Velocity Distribution

Development of the flow in the double-offset Y-shaped aircraft intake duct with equal offsets of 22.5/22.5 deg is presented in the form of isocontours of the normalized longitudinal velocity u_a/u_μ and the crossflow u_{yz}/u_μ vector plots at a Reynolds number of 1.35×10^5.

Longitudinal velocity distribution at selected planes (Fig. 5) shows the shift of the core flow along the diagonal plane, with magnitude of $0.90u_\infty$ at plane 1. Core flow is seen closer to the inner wall as an effect of the centrifugal force imposed by the curvature and the vertical offset. A small region of the flow reversal is seen at the top corner of plane 2. The region of flow reversal increases as the flow moves downstream in the duct, with the core flow moving continuously toward the bottom of the plane along the diagonal. At the inflexion plane, the size of the flow reversal still increases, with movement of the core flow still toward the downward direction. It is also seen that the flow very close to the curved wall has a tendency to move upward toward the upper corner. This phenomenon is clearly visible after the inflexion plane, in which a reverse-flow pocket has moved downward along the inner wall and flow is seen along the longitudinal direction in the top corner (plane 3). Further, there is a change in the shape of the contours close to the top corner, which can be due to a change in the direction of the centrifugal force as a result of reversal in the geometrical curvature. This phenomenon continues beyond plane 3, with higher flow taking place in the upper zone. Similar observations were made by Chyu and Bencze [24] in the case of a rectangular-to-circular transition duct. At the merging plane, a detached separated reverse-flow zone can be observed that is double the size of that of the reverse pocket seen in the previous plane, with flow remaining symmetric about the longitudinal plane. The core flow has a maximum velocity of $0.85u_\infty$, whereas the highest negative velocity is on the order of $0.05u_\infty$. Isocontours of longitudinal velocity at the outlet show the recovery of flow in the straight section and the absence of a flow-reversal pocket. The maximum velocity at this plane is found to be $0.80u_\infty$. The flow recovery beyond the merging plane highlights the role of the nondiffusing straight duct.

The flow in the double-offset Y diffusing duct is quite complex in comparison with the single-offset Y duct. In the latter case, earlier studies [13–15] showed that the core flow moves toward the convex wall in the first bend and it does not change its direction of movement in the second bend, in spite of a change in direction of centrifugal force. For a double-offset diffuser, similar characteristics were seen, except that the core movement is about the diagonal plane, which is inclined at 45 deg to the abscissa. A similar observation was made by Singh et al. [16] for a double-offset S duct.

Secondary flow is a vital flow parameter and has been calculated as follows to show the normalized crossflow distribution:

$$V_{yz} = \sqrt{V_y^2 + V_z^2}/u_\infty$$

Vector plots of the secondary-flow distribution in various planes are depicted in Fig. 6. Generation of the secondary flow is seen beyond the inlet plane and its magnitude also increases with progress of the flow in the duct. A vortex is also seen in the upper corner at plane 1 and it is shifting in the diagonal plane. At plane 2, the magnitude of the crossflow increases with a change in the direction of the flow toward the curved wall, resulting in the formation of a bigger vortex parallel to the small vortex in the upper corner. The intensity of the secondary flow ($0.32u_\infty$) is higher than that at the plane 1 ($0.13u_\infty$). Further, the intensity of the crossflow increases continuously.

Vortices are clearly observed, with the flow pattern being almost similar to that at the inflexion plane, with slightly less intensity. At plane 4, two pairs of vortices are clearly visible. The formation of two pairs of vortices may be a result of the strong interaction of centrifugal force, geometry of the curvature, and radial pressure gradient. The crossflow split about the 45-deg diagonal can be due to the same phenomenon. At the merging plane, four pairs of the counter-rotating vortices are clearly seen (two in each limb), with one pair from each limb being smaller than the other pair. The position of these vortices is along two chords with rather small gaps. The secondary-flow pattern at the outlet is almost similar to that at the merging plane, and the only difference is in the intensity of the crossflow ($0.09u_\infty$). In addition, a pair of Dean-type vortices are also visible near the side wall at the outlet of the duct (see the exploded view in Fig. 6g). The presence of these types of vortices is due to the double inflexion in the curvature. Foster et al. [25] also observed the high intensity of secondary flow in a rectangular-to-semicircular transition S duct.

Similar observations were reported by the other researchers [13–15] for a single-offset Y duct; the only difference is in the intensity of the secondary flow and the presence of an additional pair of vortices.

B. Effect of Vertical Offset

CFD analyses were carried out for different vertical offsets (0/0, 15/15, 22.5/22.5, and 30/30 deg) for a fixed horizontal offset (22.5/22.5 deg) to study the effect of the vertical offset on the performance and flow characteristics of the double-offset Y duct.

Longitudinal velocity distributions at the merging plane of the Y ducts for three vertical offsets with a fixed horizontal offset (22.5/22.5 deg) at a Reynolds number of 1.35×10^5 are presented on the left in Fig. 7. Contours are symmetric about the midvertical plane and the flow reversal is not seen for the duct without a vertical offset. The core flow from both limbs spreads in the outward direction at the merging plane. With the imposition of a vertical offset, flow starts to shift toward the bottom wall along the diagonal planes. The longitudinal velocity distribution at the merging plane for a Y duct with a 15/15-deg vertical offset (Fig. 7b) shows that the core flow moves downward and it is inclined with the diagonal plane at an angle of 30 deg to the vertical. The low-velocity region is confined at the top and flow reversal is also seen there. Similar observations were made by other researchers [13–15] for the Y duct without a vertical

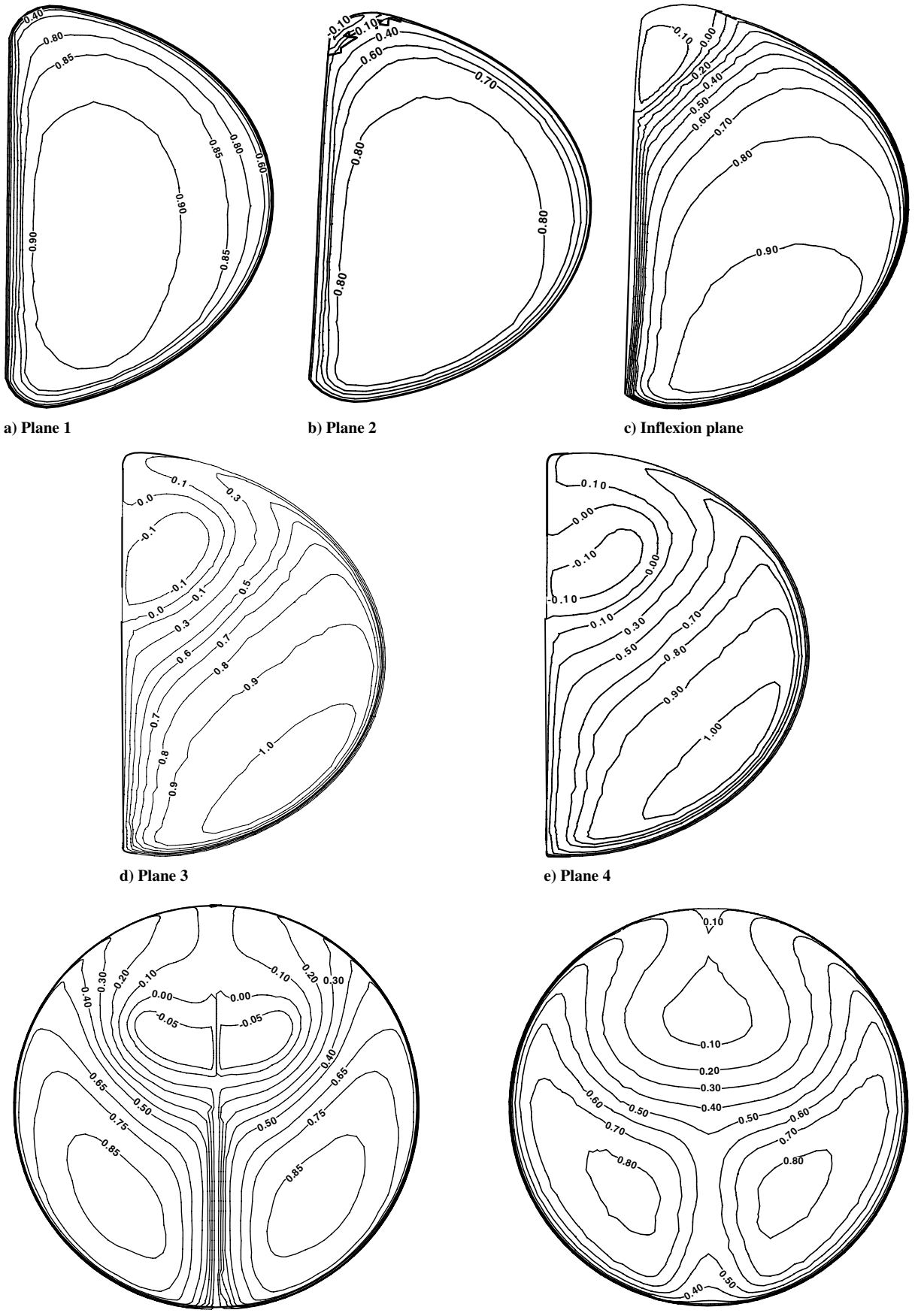

Fig. 5 Normalized longitudinal distribution at various selected planes of a double-offset Y-shaped diffuser with equal offsets (22.5/22.5 deg); $Re = 1.35 \times 10^5$.

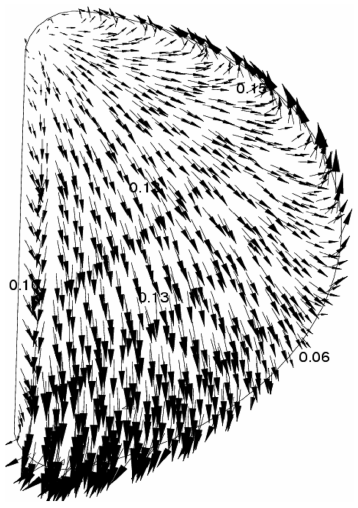

a) Plane 1

b) Plane 2

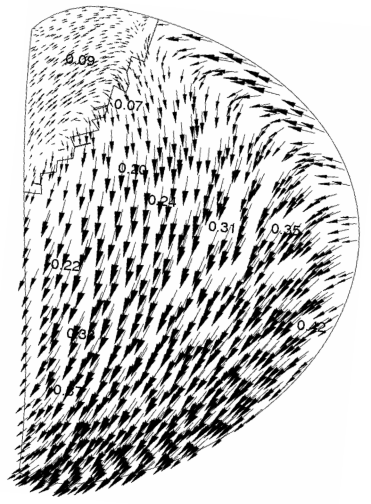

c) Inflexion plane

d) Plane 3

e) Plane 4

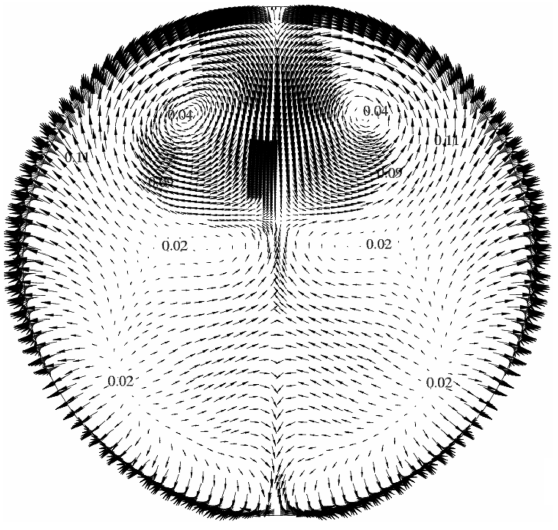

f) Merging plane

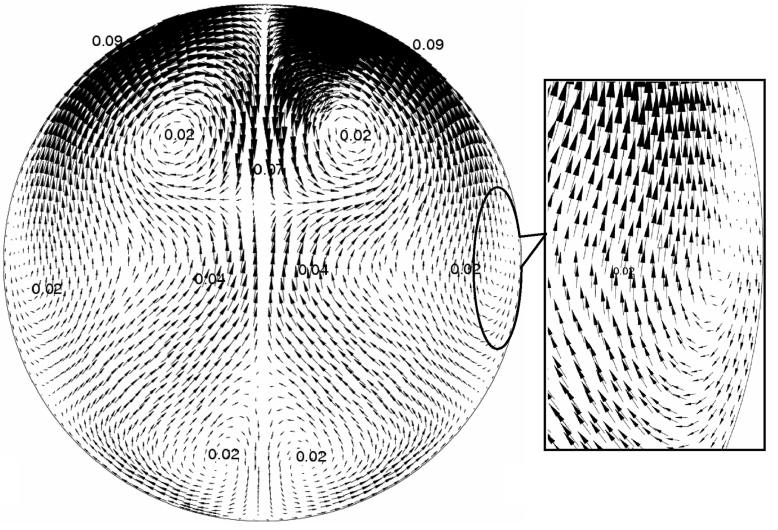

g) Outlet plane

Fig. 6 Normalized vector plots of secondary flow at various selected planes of a double-offset Y-shaped intake duct with equal offsets (22.5/22.5 deg); $Re = 1.35 \times 10^5$.

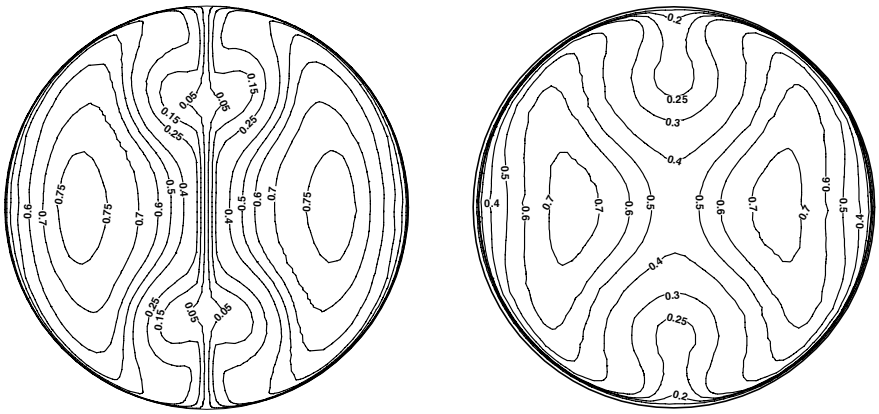

a) No vertical offset

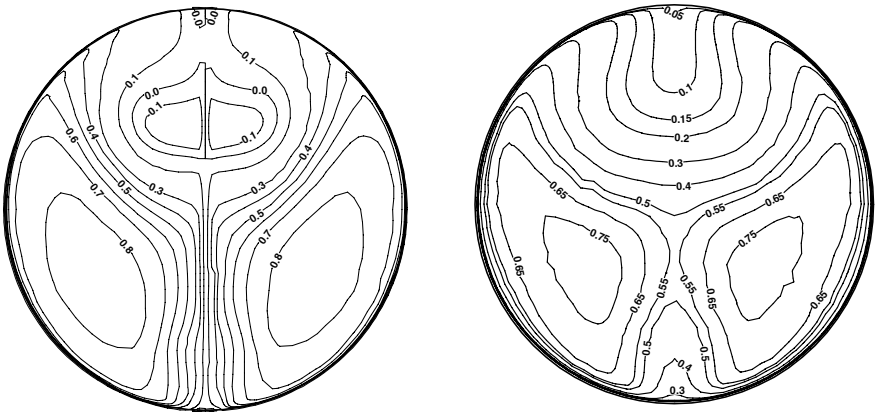

b) Vertical offset: 15°/15°

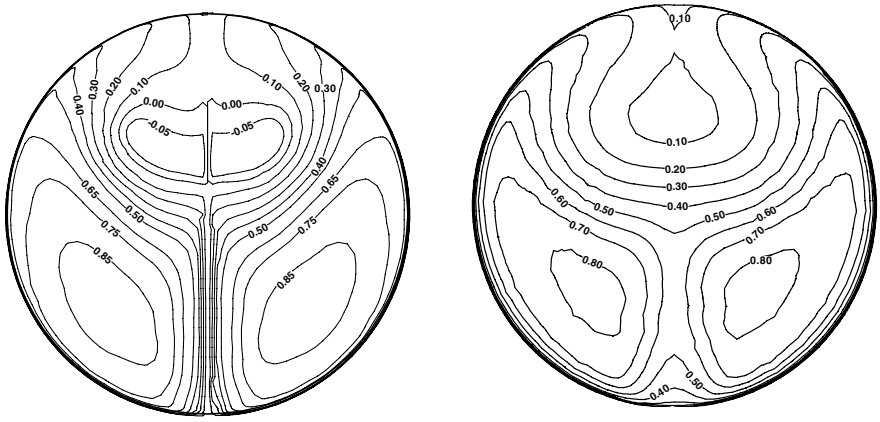

c) Vertical offset: 22.5°/22.5°

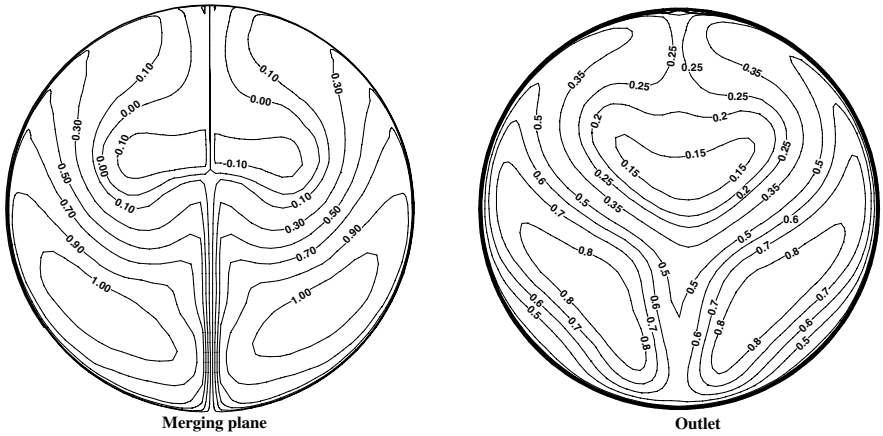

d) Vertical offset: 30°/30°

Fig. 7 Longitudinal velocity distribution in two planes of the Y ducts with a fixed horizontal offset (22.5/22.5 deg) and different vertical offsets.

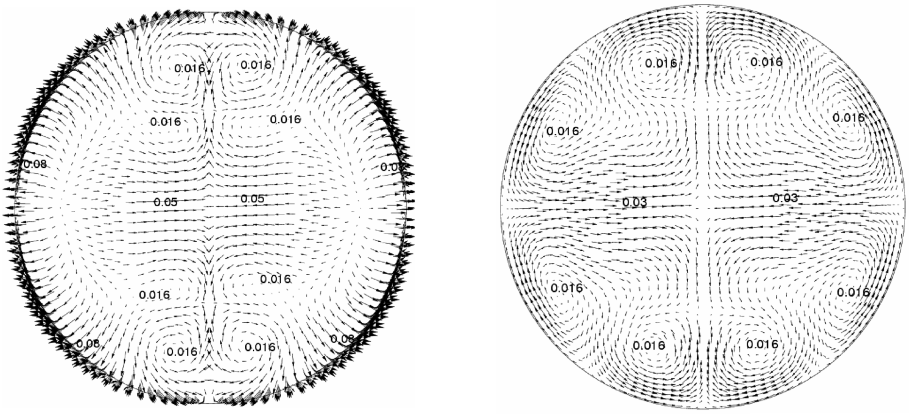

a) No vertical offset

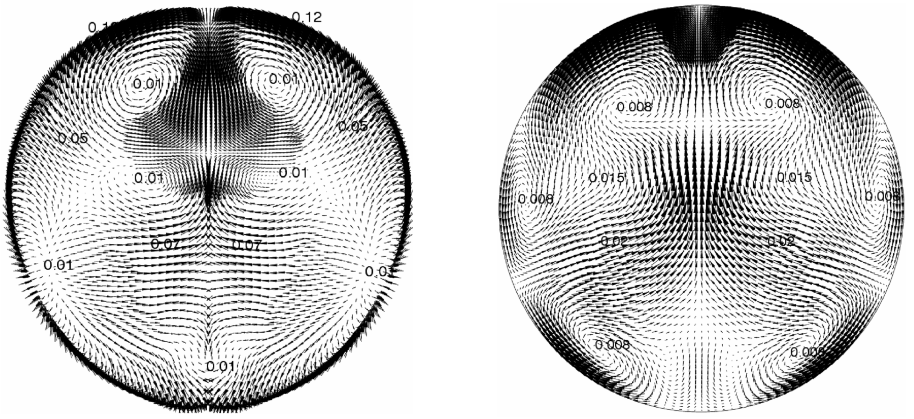

b) Vertical offset 15°/15°

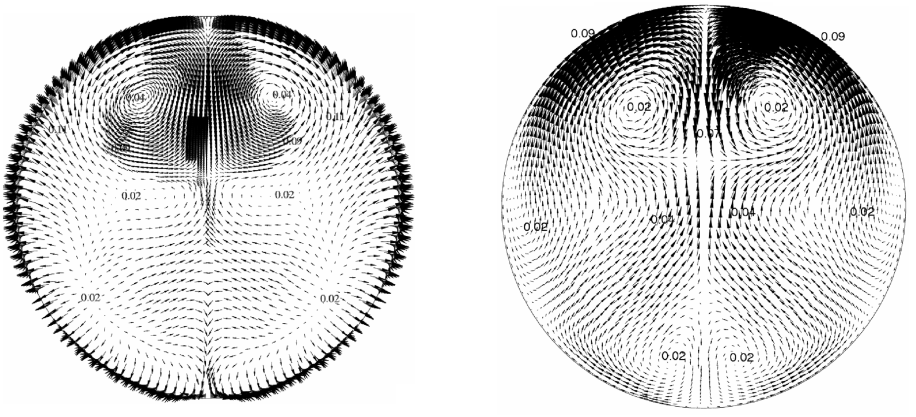

c) Vertical offset 22.5°/22.5°

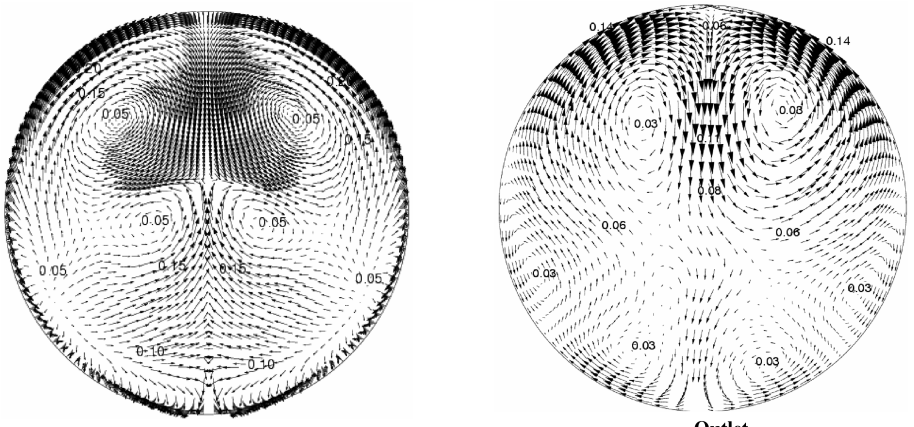

Merging Plane Outlet

d) Vertical offset 30°/30°

Fig. 8 Secondary-flow distribution at $Re = 1.35 \times 10^5$ for a Y duct with a fixed horizontal offset (22.5/22.5 deg) and different vertical offsets.

offset. Velocity distribution at the merging plane for the duct with a 22.5/22.5-deg vertical offset has already been discussed in the previous section. For a 30/30-deg vertical offset (Fig. 7d), core flow moves in the downward direction and it is located in a diagonal plane that is inclined at 60 deg to the vertical axis. Size of the recirculation zone increases further there by forcing the flow toward the bottom as a result of additional centrifugal force caused by the higher vertical offset. The shape of contours has a tendency to become more concave at the upper section, due to an enlarged flow-reversal zone. It is also observed that the velocity in the core flow has a maximum value of $1.05u_\infty$ for the 30/30-deg vertical offset, whereas its value is $0.90u_\infty$ for the 15/15-deg duct. Further, it is also observed that the reverse flow has a maximum value for the case of a 30/30-deg vertical offset, whereas 15/15 deg has the least value.

The longitudinal velocity distribution at the exit of the ducts shown on the right in Fig. 7 shows the recovery of the flow downstream of the merging plane and that the size of the reverse flow starts to reduce. Flow distribution seems to be more uniform at the exit than at the merging plane. Flow distribution is seen to be most disturbed for the 30/30-deg vertical offset. Similar flow features were reported by Singh et al. [16] for double-offset S ducts.

Secondary-flow distribution at the merging plane for Y ducts are presented as vector plots in Fig. 8 (left side), which clearly shows the presence of two pairs of counter-rotating vortices at the merging plane. For a Y duct without a vertical offset, two pairs of counter-rotating vortices are seen close to the wall, placed symmetrically along the vertical diagonal (Fig. 8, left side). Similar observations were reported by other researchers [13,14]. The effect of the vertical offset can be clearly seen by observing Figs. 8b–8d . With an increase in the vertical offset, two pairs of the vortices become asymmetric and the intensity of one pair of vortices increases, whereas that of the other pair reduces. This could be due to the presence of a second curvature, which results in higher centrifugal force and the reorientation of the plane along which the centrifugal force acts. The intensity of the secondary flow is seen to be the highest ($0.20u_\infty$) for the 30/30-deg vertical offset, whereas 15/15 deg has the lowest value ($0.11u_\infty$). With an increase in the vertical offset, the intensity of the crossflow at the center also increases (0.03, 0.07, 0.11, and 0.15 for zero offset and 15/15, 22.5/22.5, and 30/30 deg, respectively). Similar observations were also reported by Singh et al. [16] for a double-offset S duct, in which vortices also shift to the diagonal plane.

The secondary velocity distribution at the exit is shown in Fig. 8 (right side), and it is seen that the intensity of the secondary flow reduces, due to the recovery of flow in the straight section of the duct. The features of the vector plots are almost similar to those at the merging plane. The differences in the secondary-flow pattern observed at this plane are that the vortices have started moving toward the top wall and an additional pair of vortices, similar to Dean-type vortices, is observed near the side wall.

The performance characteristics in terms of the coefficient of pressure recovery C_P, pressure-loss coefficient C_L, and the distortion coefficient DC_{60} were evaluated for the intake duct. C_P and C_L are defined as

$$C_P = \frac{p_{si} - p_{so}}{\frac{1}{2}\rho U_{in}^2} \qquad C_L = \frac{p_{Ti} - p_{To}}{\frac{1}{2}\rho U_{in}^2}$$

Figure 9a shows the variation of the coefficient of pressure recovery C_P in the longitudinal direction for different vertical offsets. A Y duct without a vertical offset has the highest value of overall C_P (0.60). C_P increases continuously in the longitudinal direction up to the exit, except in the region near the inflexion plane, as a result of loss due to flow separation in this region. Observing the variation of C_P for different vertical offsets, the variation of C_P is nearly the same for all ducts up to the plane 1, which exhibits reasonably faster diffusion. Further downstream, there is a drop in the value of C_P up to the inflexion plane, which can be attributed to the flow separation and higher intensity of the secondary flows. The drop of C_P is higher for larger vertical offsets. After the inflexion plane, C_P again increases

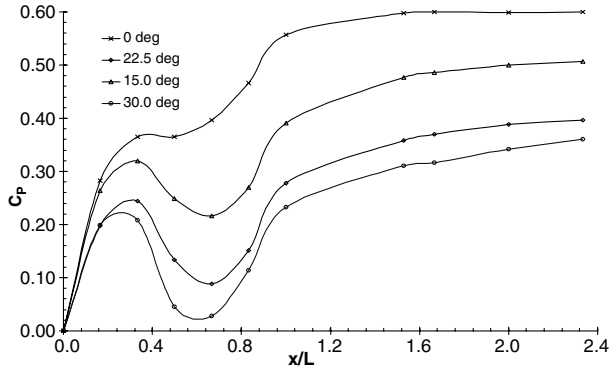

a) Variation of coefficient of pressure recovery

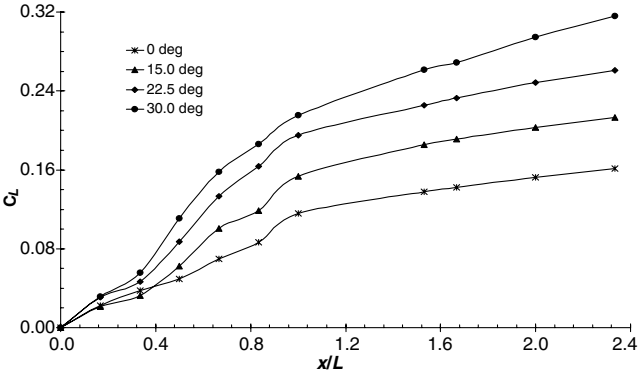

b) Variation of total pressure loss coefficient

Fig. 9 Variation of performance parameters with a vertical offset for a Y duct with fixed horizontal offset (22.5/22.5 deg) .

up to the merging plane and pressure recovery is slow thereafter. An increase in the value of C_P in the straight duct is due to the flow development in that section. The duct with the largest vertical offset (30/30 deg) has the least value of C_P (0.36). Computed values of overall C_P for different vertical offsets are given in tabular form in Table 2.

The variation of C_L for various vertical offsets is shown in Fig. 9b. The intake duct with a 30/30-deg vertical offset has the highest loss coefficient (0.32), whereas the duct with a 15/15-deg vertical offset has a lower loss coefficient (0.21). C_L for the duct without a vertical offset has the least value of C_L (0.16). Higher losses in the duct with a vertical offset are due to an increase in secondary flow and flow separation.

The performance of the aircraft engine is highly influenced by the flow distortion at the exit of the intake duct. This condition is quantified by the total pressure distribution at the exit and by the distortion coefficient [12]. This is calculated as

$$\mathrm{DC}(\theta) = \frac{p_f - p_\theta}{\frac{1}{2}\rho v_e^2}$$

where p_f is the mean total pressure at the exit of the duct, p_θ is the mean total pressure in the worst sector at the exit of the duct, which is invariably taken as 60 deg [12], and v_e is the mean velocity at the exit. Computed values of the distortion coefficient DC_{60} for different vertical offsets are given in Table 2. It is seen that the value of DC_{60}

Table 2 Effect of a vertical offset on the performance of a double-offset Y duct with a fixed horizontal offset of 22.5/22.5 deg

Vertical offset	C_P	C_L	DC_{60}
No offset	0.60	0.16	0.61
15/15 deg	0.51	0.21	0.90
22.5/22.5 deg	0.40	0.26	0.96
30/30 deg	0.36	0.32	0.96

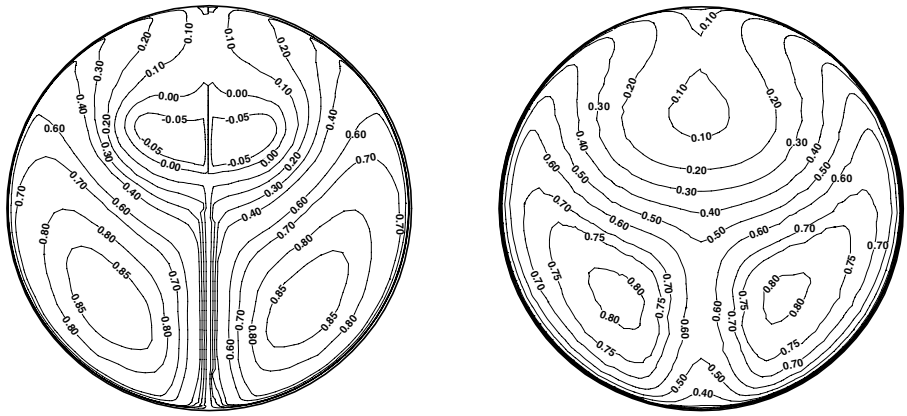

a) Re=4.5x10^4

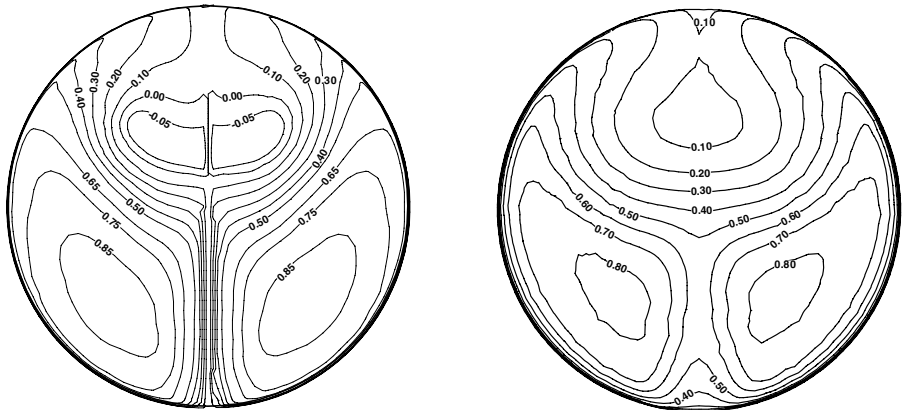

b) Re=1.35x10^5

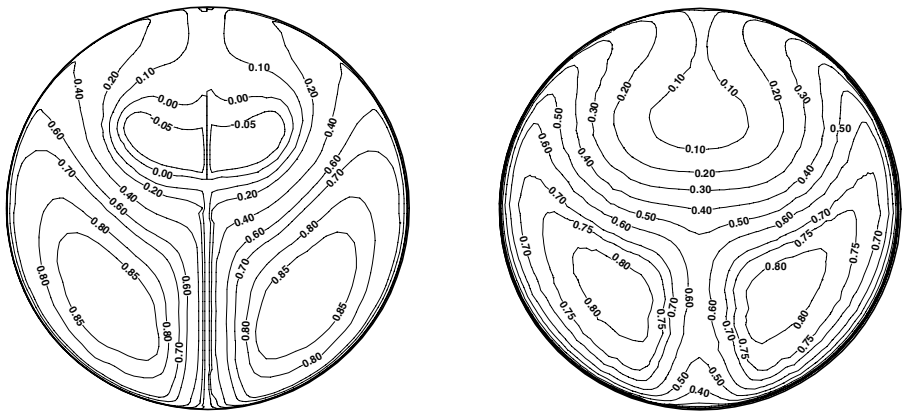

c) Re=2.70x10^5

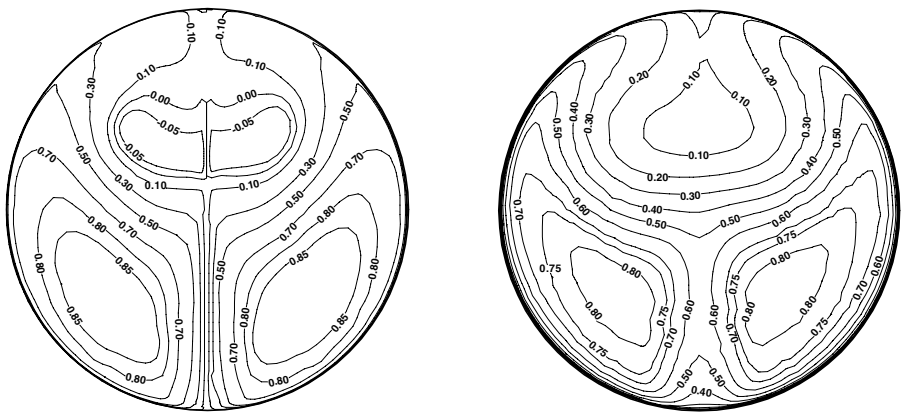

Merging plane Exit

d) Re=4.05x10^5

Fig. 10 Effect of Reynolds number on the longitudinal velocity distribution for a Y duct with equal offsets (vertical and horizontal offset of 22.5/ 22.5 deg).

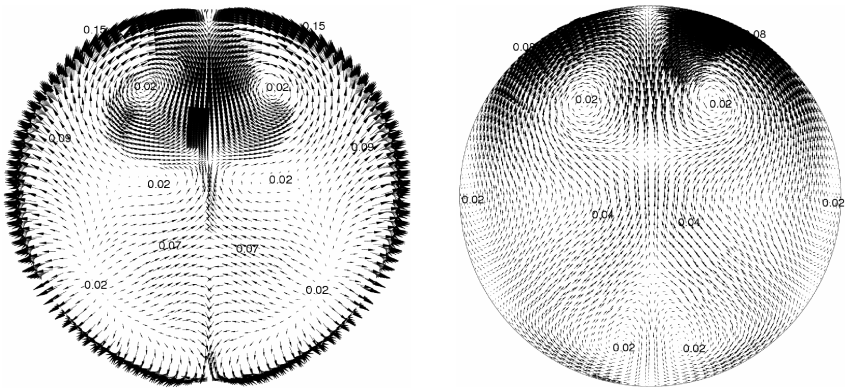

a) Re = 4.50x10^4

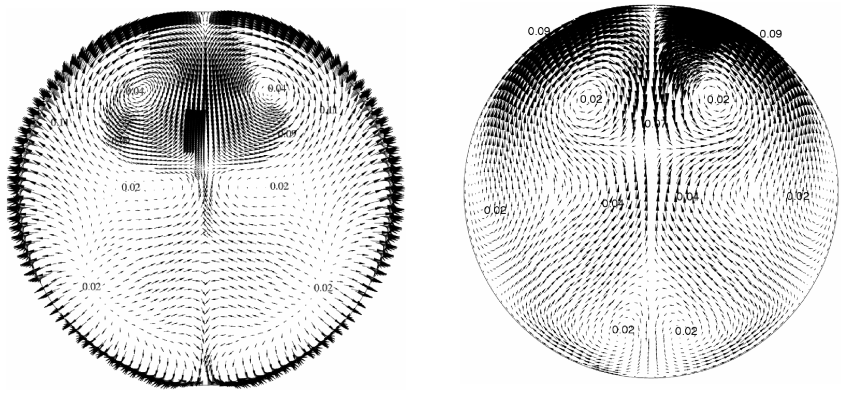

b) Re = 1.35x10^5

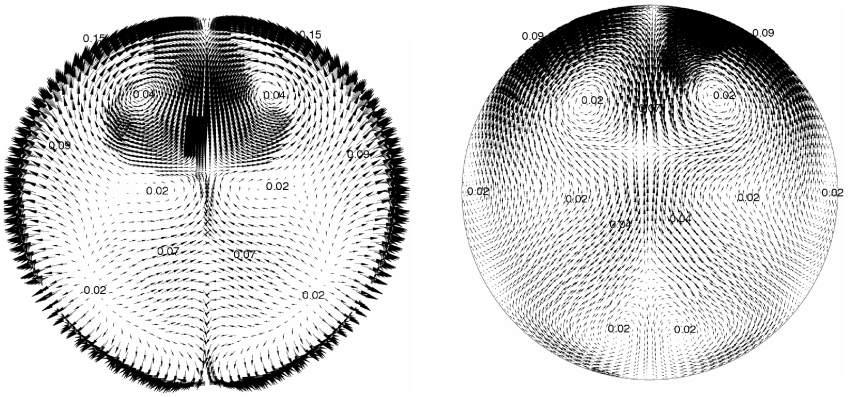

c) Re = 1.35x10^5

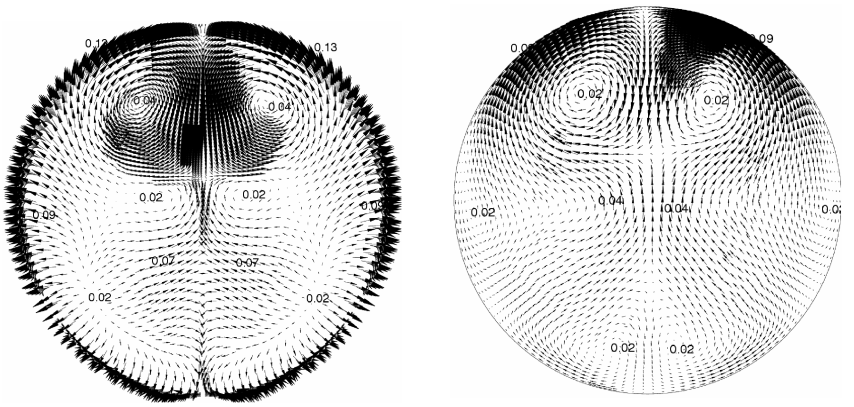

Merging Plane Exit

d) Re = 4.05x10^5

Fig. 11 Effect of Reynolds number on the crossflow distribution for a Y duct with equal offsets (vertical and horizontal offset of 22.5/22.5 deg).

increases drastically with the introduction of a vertical offset, which implies the reduction of flow uniformity at the exit. A duct with zero vertical offset has the least value (0.61), whereas a diffuser with a 15/15-deg vertical offset has a DC_{60} value of 0.90. Slightly higher values of distortion coefficient for the case of higher offsets can be due to larger regions of flow reversal and generation of the strong secondary flows at the inflexion plane.

C. Effect of Reynolds Number

A Y duct with equal offsets (both horizontal and vertical offsets are 22.5/22.5 deg) was chosen to study the effect of Reynolds number on the performance of a double-offset Y duct. The longitudinal velocity distributions at the merging plane of the Y-shaped intake duct at four Reynolds numbers are shown on the left in Fig. 10. It is seen that the Reynolds number does not have a significant effect on the flow characteristics. The flow pattern at the merging plane is almost identical for all cases. The maximum value of velocities in the region of the flow reversal ($-0.05u_\infty$) and the core flow ($0.85u_\infty$) are the same in all cases. Similar observations were made by Bharani et al. [12] for a Y duct with zero vertical offset. Singh et al. [16] also showed that the performance of a double-offset S duct is independent of the Reynolds number at higher ranges ($Re > 10^5$).

Longitudinal velocity contours at the outlet presented on the right in Fig. 10 show the flow patterns to be almost similar to those at the merging plane, with improved flow uniformity in all cases. The detached reverse-flow pocket present at the merging plane near the top wall has disappeared at the exit plane, showing the improvement in flow quality. The maximum velocity ($0.80u_\infty$) in the core flow is also the same for all cases.

Normalized crossflow distribution in the merging plane for the duct is presented on the left in Fig. 11. Two pairs of the contrarotating vortices exist at the merging plane, with the intensity of one pair being higher. Further, it is seen that the pattern of secondary flow is similar at all Reynolds numbers. The lowest values of crossflow are seen close to the top wall at the Reynolds number of 4.5×10^4, whereas at higher Reynolds numbers, magnitudes of the secondary flow are almost the same.

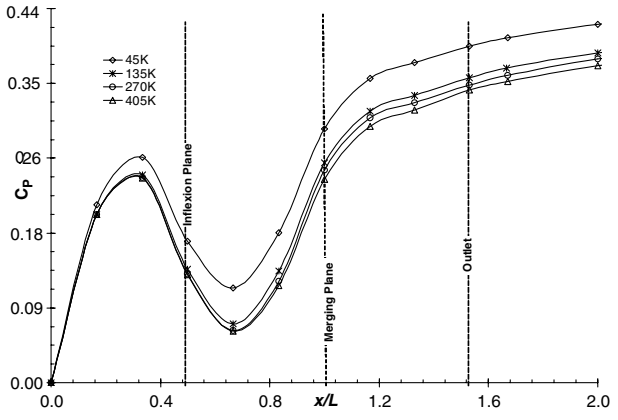

a) Variation of coefficient of pressure recovery

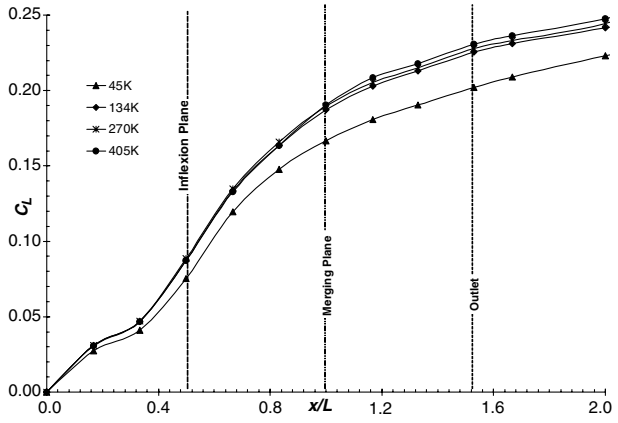

b)Variation of total pressure loss coefficient

Fig. 12 Variation of performance parameters at different Reynolds numbers for a Y duct with equal offsets (vertical and horizontal offset of 22.5/22.5 deg).

Table 3 Effect of the inlet Reynolds number on the performance of a double-offset Y duct with equal offsets of 22.5/22.5 deg

Reynolds number	C_P	C_L	DC_{60}
4.45×10^4	0.43	0.22	0.958
1.35×10^5	0.40	0.25	0.960
2.70×10^5	0.39	0.25	0.961
4.05×10^5	0.38	0.25	0.961

Crossflow vector plots at the exit of the ducts for different Reynolds numbers are shown on the right in Fig. 11. It is seen that the recovery of flow continues and smaller vortices are observed. In addition to the smaller vortices, a pair of Dean-type vortices is also observed on both sides of the exit plane. Further, the intensity of the secondary flow is lower than that at the merging plane. The flow pattern and the intensity of the secondary flow are almost identical for all cases. A similar observation was reported for a double-offset diffusing S duct [16].

The variations of the coefficient of static pressure recovery at different Reynolds numbers are shown in Fig 12a. Trends of the coefficient of pressure-recovery variation are similar at all Reynolds numbers. It is further observed that the variation of C_P is nearly the same up to plane 1 in all cases. After this plane, the value of C_P reduces up to the inflexion plane. Beyond the inflexion plane, the values of C_P increase continuously. Reduction in the value of C_P up to the inflexion plane is due to the generation of strong secondary flows caused by the interaction of centrifugal force and radial pressure gradient. A higher recovery rate is seen in the region between plane 3 and the merging plane. It is also seen that flow continues to recover beyond the merging plane with a lower recovery rate. The highest value of C_P (0.43) is at the lowest Reynolds number of 4.50×10^4, whereas at higher Reynolds numbers, the overall value of C_P is nearly constant (0.39).

Variations of the total-pressure-loss coefficient at various Reynolds numbers are presented in Fig. 12b. The loss coefficient increases continuously up to the exit plane, except in a small region close to the plane 1, in which it increases marginally. Further, it is also observed that the rate of increase in the loss coefficient reduces beyond the merging plane. Computed values of overall C_L at various Reynolds numbers are given in Table 3. It is seen that Reynolds number has no significant effect on the value of C_L for Reynolds numbers higher than 10^5.

Computed values of distortion coefficients DC_{60} at various Reynolds numbers are given in Table 3. It is seen that DC_{60} has a value of 0.958 at a lower Reynolds number (4.50×10^4), whereas its value is found to be almost constant (0.961) at higher Reynolds numbers ($Re > 10^5$). From the values of DC_{60}, it can be concluded that the Reynolds number has no significant effect on the flow uniformity at the exit of the duct.

VI. Conclusions

Performance characteristics of double-offset Y-shaped aircraft intake ducts were investigated using the RNG k-ε turbulence model. The following significant observations were made:

1) Velocity distribution at the exit of the duct shows the movement of the core of the flow along the 45-deg diagonal for equal offsets of 22.5/22.5 deg. The angular shift of the diagonal plane also depends on the magnitude of the vertical offset (30 deg for the 15/15-deg and 60 deg for the 30/30-deg vertical offsets).

2) Secondary-flow distribution in the merging plane shows the formation of two pairs of counter-rotating vortices, for which the intensity reduces at the exit of the duct. The intensity of the secondary

flow is higher than that with a single-offset Y duct. A pair of Dean-type corner vortices is also observed at the exit.

3) The flow characteristics are nearly independent of the Reynolds number if its value is higher than 10^5.

4) The performance of the Y duct with a double offset deteriorates significantly with increasing vertical offset, and hence only mild curvatures (up to 15/15 deg) should be chosen, as much as possible.

References

[1] Whitford, R., *Design for Air Combat*, Jane's, London, 1987.

[2] Martin, N. J., and Holzhauser, C. A., "An Experimental Investigation at Large Scale of Single and Twin NACA Submerged Side Intake at Several Angles of Side Slips," NACA RM A9F20, 1949.

[3] Martin, N. J., and Holzhauser, C. A., "An Experimental Investigation at Large Scale of an NACA Submerged Intake and Deflector Installation on the Rearward Portion of a Fuselage," NASA RM A50F13, 1950.

[4] Jolly, R., Pai, T. G., and Jayasimha, P., *Design and Development of a Bifurcated Y Duct Intake for a Modern Combat Aircraft*, Hindustan Aeronautics Ltd., Bangalore, India, 1996.

[5] Pai, T. G., *Aerodynamic Testing of Air Intake for a Modern Combat Aircraft*, Aeronautical Development Agency, Bangalore, India, 1994.

[6] Sudhakar, K., and Ananthkishnan, N., "Jump Phenomenon in Y-Shaped Intake Ducts," *Journal of Aircraft*, Vol. 33, No. 2, 1995, pp. 438–439.

[7] Obery, L. J., and Cubbison, R. W., "Effectiveness of Boundary Layer Removal Near Throat of Ramp Type Side Inlet at Freestream Mach Number of 2.0," NACA RM-E54I14, 1954.

[8] Obery, L. J., and Stitt, L. E., "Investigation at Mach Number 1.5 and 1.7 of Twin Duct Side Air Intake system with 9° Compression Ramp Including Modifications to Boundary Layer Removal Wedge and Effect of Bypass System," NACA RM E53H04, Oct. 1953.

[9] Davis, W. F., and Goldstein, D. L., "Experimental Investigation at Supersonic Speeds of Twin Scoop Duct Inlets of Equal Area, 2: Effect of Slot upon an Inlet Enclosed 61.5 Percent of the Maximum Circumference of the Forebody," NACA RM-A8C11, June 1948.

[10] Davids, J., and Wise, G. A., "Investigation at Mach Number 1.5 and 1.7 of Twin Duct Side Air Intake System with 6° Compression Ramp Mounted on a Supersonic Airplane," NACA RM E53H19, 1953.

[11] Seddon, J., and Goldsmith, E. L., *Intake Aerodynamics*, 2nd ed., Blackwell Science, London, 1999.

[12] Bharani, S., Singh, S. N., Seshadri, V., and Chandramouli, R., "Performance Evaluation of Divided Intake Duct: Effect of Area Ratio and Inlet Reynolds Number," *International Journal of Fluid Mechanics Research*, Vol. 30, No. 5, 2003, pp. 525–541. doi:10.1615/InterJFluidMechRes.v30.i5.60

[13] Bharani, S., Singh, S. N., Seshadri, V., and Chandramouli, R., "Effect of Angle of Turn on the Performance of Divided Intake Ducts," *Proceedings of the Institution of Mechanical Engineers, Part G (Journal of Aerospace Engineering)*, Vol. 218, No. 1, 2004, pp. 23–31.

[14] Patel, T., Singh, S. N., and Seshadri, V., "Characteristics of Y-Shaped Rectangular Diffusing Duct at Different Inflow Conditions" *Journal of Aircraft*, Vol. 42, No. 1, Jan.–Feb. 2005, pp. 113–120. doi:10.2514/1.4690

[15] Saha, K., Singh, S. N., and Seshadri, V., "Influence of Inlet Shape on Twin Intake Duct Performance," *Turbo Expo 2005*, American Society of Mechanical Engineers Paper GT2005-68056, June 2005.

[16] Singh, R. K., Singh, S. N., and Seshadri, V., "Flow Characteristics of a Double-Offset S-Shaped Circular Diffusing Duct," *International Journal of Fluid Mechanics Research*, (to be published).

[17] Hinze, J. O., *Turbulence*, 6th ed., McGraw–Hill, New York 1975.

[18] Yahkot, V., and Orszag, S. S. "Renormalization Group Analysis of Turbulence, 1: Basic Theory," *Journal of Scientific Computing*, Vol. 1, No. 1, 1996, pp. 1–51.

[19] Ferzieger, J. H., and Peric, M., *Computational Method for Fluid Dynamics*, 3rd ed., Springer–Verlag, Berlin, 2000.

[20] FLUENT, Software Package, Ver. 6.2, Fluent, Inc., Lebanon, NH, 2002.

[21] Patankar, S. V., *Numerical Heat Transfer and Fluid Flow*, Taylor and Francis, London, 1980.

[22] Anand, R. B., "Flow Through S-Shaped Diffusing Ducts," Ph.D. Thesis, Dept. of Mechanical Engineering, Indian Inst. of Technology Delhi, New Delhi, India, 2002.

[23] Fox, R. W., and Kline, S. J., "Flow Regime in Curved Subsonic Diffuser," *Journal of Basic Engineering*, Vol. 84, Sept. 1962, pp. 303–316.

[24] Chyu, W. J., and Bencze, D. P. "Navier-Stokes Simulation of Flow Through a Highly Contoured Subsonic Diffuser," *International Journal for Numerical Methods in Engineering*, Vol. 34, No. 2, 1992, pp. 473–483. doi:10.1002/nme.1620340207

[25] Foster, J., Wendt, B. J., Reichert, B. A., and Okiishi, T. H., "Flow Through a Rectangular to Semiannular Transition Duct," *Journal of Propulsion and Power*, Vol. 13, No. 2, 1997, pp. 312–317.